3D SCANNING AS AN EFFECTIVE TOOL FOR CONTROLLING THE DIMENSIONS OF TEST SPECIMENS

Michal VYHLÍDAL[1]

[1]Institute of Structural Mechanics, Faculty of Civil Engineering, Brno University of Technology, Veveří 331/95, 602 00 Brno, Czech Republic

vyhlidal.m@fce.vutbr.cz

DOI: 10.35181/tces-2022-0014

Abstract. *3D laser scanning is a powerfull tool that digitally captures the shape of physical objects using a laser light crosses. In this work, the 3D laser scanning technology is used for the 3D shape capture of specially designed specimens. These specimens previously made of fine-grained cement-based composite of the nominal dimensions* $40 \times 40 \times 160$ *mm with inclusion in the shape of prisms with nominal dimensions of* $8 \times 8 \times 40$ *mm were provided with an initial central edge notch and tested in the threee-point bending configuration. The aim of this paper is to study the macrostructure of fracture surfaces via 3D scanning technology, measure the area of ligament, verify the designed notch depth and evaluate the fracture toughness and specific fracture energy based on the measured dimensions. The results indicate that the measured notch depth is lower than the designed one thus the differences between fracture toughness calculated for designed notch depth and for the measured one is approximately 10 %. In addition, the fracture toughness is overestimated when considering the design values.*

Keywords

3D scanning, fracture test, fracture toughness, specific fracture energy.

1. Introduction

Concrete structures such as highway bridges, tunnels, dams, etc. are important parts of the infrastructure which should serve for many generations after their construction. Traditionally, these structures are designed using a procedure mentioned in standards, e. g. EN 1992-1-1 [1], which are based on the theory of elasticity which consider volume as continuous. Nevertheless, concrete contains variety of micro- and macro-defects, inclusions etc. even at the production stage and thus methods of Fracture Mechanics is suitable to be applied. Because mechanical fracture parameters of material depend on the geometry of test specimen, configuration of fracture test, the dimension and position of stress concentrators, etc. the knowledge of all these parameters as closely as possible is necessary.

The aim of this paper is to show the fracture surfaces of previously tested specimens by 3D scanning technology, verify designed dimensions of specimens and evaluate the selected mechanical fracture parameters according to the measured dimensions.

2. Theoretical background

2.1. Interface shear transfer

The bond mechanism in concrete is a result of the interaction between aggregate grain and matrix. Bond resistance is a combination of mechanical interlocking, friction and chemical adhesion. The mechanical interlocking resistance takes place in the case of excessive and irregular roughness, while the frictional resistance is a result of the compression forces acting perpendicular to the interface and depends on the degree of interface roughness. Adhesive resistance is a result of chemical and physical bonding due to Van der Waals forces and is in the range of lower units of MPa for concrete grades $\leq$ C50/60. Adhesive resistance strongly depends on the real surface of the contact area, and the quality, composition and properties (mainly porosity) of concrete [2, 3].

2.2. 3D scanning technology

In recent years, 3D scanning technology has been widely used mainly in the mechanical engineering industry to control the accuracy and quality of products. The main advantages in compared to conventional measurement methods is higher accuracy, speed and reliability [4, 5, 6].

There are a variety of technologies for digitally acquiring shape of a 3D object, but in general it can be divided into two types – contact and non-contact [5]. In this paper, a non-contact type is used, so attention is paid only to this. The principle of 3D laser scanning technology consists in the projection of a laser beam by a laser emitter onto the surface of the scanned object and the simultaneous scanning of these projected beams by a high-speed camera/s located in the 3D scanner. The process of the coordinate calculation uses the triangulation principle. The triangulation principle is based on the observation of a point from two different stations. These two stations and scanning point define a triangle. With the knowledge of the distance between these two stations (focal distance) and defining the angles of the projection ray and of the camera/s, the coordinates of the intersection point can be calculated from the triangle [4, 5, 6].

The process of identifying the coordinates of a point A (and others) begins with the camera image processing, more precisely by finding the projected laser beam in the camera image. The result is the image coordinates (x_k, y_k) of the image A' of a point A in the local coordinate system of the camera. Subsequently, the spatial coordinates (x, y, z) of point A can be calculated using triangulation. However, these are not the absolute coordinates of point A, but the coordinates in the scanner's local coordinate system. To scan the surfaces of larger objects, or their parts, it is necessary to change the position of the scanner, which leads to a redefinition of the local coordinate system, which no longer corresponds to the original coordinate system. The transformation of the coordinates to the absolute ones or to track the scanner's position is mandatory for the proper scanning [4, 5, 6].

The scanner's position is determined based on the technology of positioning targets, which track the position of the scanner in space in relation to the part being scanned. These targets are a small cicular black-and-white stickers, which are placed directly on the part or in its close vicinity. The first stage of scanning consist of the reference points identification (principle similar to the stereo vision). Each image needs a minimum of 4 targets in the field of view to be aligned. The next stage is the projection of the laser cross together with the recalculation of the coordinates into the global coordinate system [4, 5, 6].

The result is a 3D coordinates of all visible points at the laser projection point which generates polygonal mesh after scanning – see Fig. 1.

Fig. 1: Polygonal mesh.

3. Experimental programme

To determine the influence of the inclusion on the fracture behavior of fine-grained cement-based composite, the special specimens were designed.

3.1. Specimens and materials

The specimens with nominal dimensions of 40 × 40 × 160 mm containing an internal inclusion with nominal dimensions of 8 × 8 × 40 mm placed in the middle of the span above the initial notch were manufactured for the fracture tests, see Fig. 2. The only difference between the test sets was the type of rock inclusion – amphibolite (AMP), basalt (BAS), granite (GRA), or marble (MAR) [7, 8].

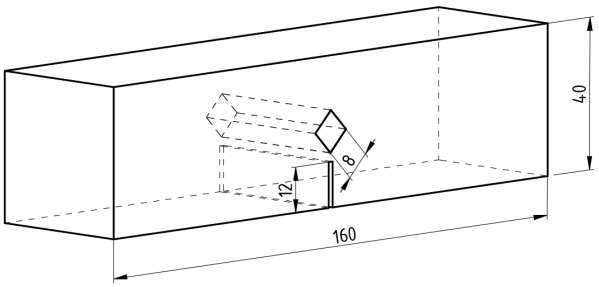

Fig. 2: Specimen geometry.

The matrix of the test specimens was prepared from a fine-grained cement-based composite. The fresh mixture consisted of CEM I 42.5 R Portland cement, standard quartz sand with a maximum grain size of 2 mm, and water in the ratio 1:3:0.35 (cement:sand:water). To ensure workability, a polycarboxylate-based high-range water-reducing admixture (Sika SVC 4035) was added in an amount of 1 % by cement mass. For more details, see [7].

3.2. Fracture tests

Fracture tests were conducted using a LabTest 6-1000 multi-purpose mechanical testing machine under monotonic loading conditions with a constant displacement increment of 0.02 mm·min^{-1}. The load span was 120 mm. During the experiment, besides the force F, vertical mid-span displacement (deflection) d and crack mouth opening displacement $CMOD$ were continuously recorded [8].

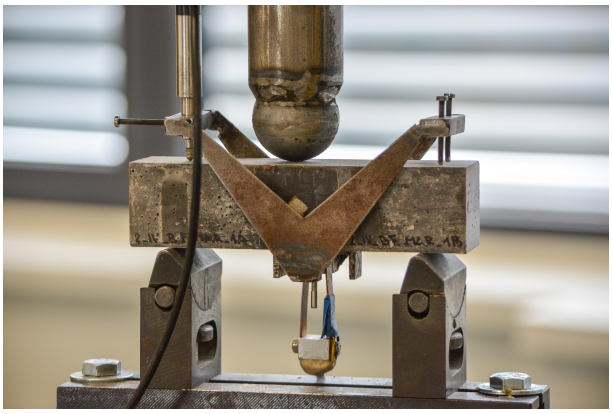

Fig. 3: Detail of measuring equipment.

3.3. Process of 3D scanning

Scanning was provided by a 3D scanner HandySCAN 700, which is provided by two highspeed cameras and 7 lasers crosses to quick capture of the entire field of view. The accuracy of scanner is up to 0.03 mm, the volumetric accuracy reachs 0.02–0.06 mm/m and a maximum resolution (length of element of polygonal mesh) is up to 0.05 mm [9].

Process of 3D scanning is very simple and consists of the following operations. First of all, the calibration of 3D scanner using special calibration board is recommended. After calibration, the scanned surface must be cleaned of grease and dirt, the glossy surfaces must be sprayed with matt gray paint and position points (targets) is sticked on the surface [9]. Fortunately, the surfaces of the test specimens were clean and matt, thus scanning went without a hitch with the usage of scanning desk equipped with targets.

4. Results

4.1. Fracture tests

The force versus deflection diagram for specimens, which fracture surfaces were scanned, can be seen together with reference specimen made only from matrix (dashed line) in Fig. 4.

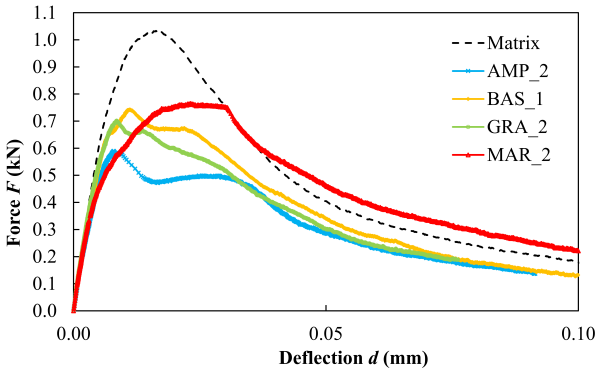

Fig. 4: The force F in (kN) vs. deflection d in (mm) diagram for scanned specimens.

The reduction of maximum force values in the case of specimens with inclusion in comparison to the reference (matrix) one is apparent. Despite that, the highest maximum force values were obtained for specimen with marble or basalt inclusion, while the lowest one for specimen with amphibolite inclusion.

4.2. Scanned fracture surfaces

In the following four figures (Figs. 5–8), the scanned specimens after fracture test are displayed. The most compact area of ligament can be seen in the case of specimens with marble (Fig. 5) and basalt (Fig. 8) inclusion. In addition, the only one monitoring crack propagation through the inclusion was observed in the case of specimen with marble inclusion, see Fig. 5. On the contrary, probably the most porous area of ligament was observed in the case of specimen with amphibolite inclusion where the horizontal alignement was also disturbed – see Fig. 7.

Advantage of 3D scanning is not only to display the macrostructure of surfaces but also to measure their dimensions. In this paper, the attention is paid to the specimen height W, edge notch depth a_0, which was designed as $0.3 \times W = 12$ mm, and area of ligament. In the following table (Tab. 1), the measured mean value of notch depth a_0 can be seen. The mean value was calculated as an area of flat surface (made by saw with diamond blade) divided by the specimen's width or it was estimated as an average value from 3 measurements (two edges and one approximately in the middle of the specimen). It is obvious that the real notch depth a_0 is lower that the designed one and thus the evaluated mechanical fracture parameters will differ from the published one's [7].

Tab. 1: Measured diamensions and areas of ligament of specimens.

Specimen	MTX	MAR	GRA	AMP	BAS
a_0 (mm)	11	10.5	10.6	10.9	10.7
W (mm)	39.8	39.9	39.8	39.9	39.9
A_{lig} (mm^2)	1298.5	1300.7	1359.4	1349.7	1291.9

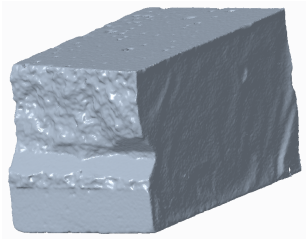

Fig. 5: Scanned surfaces of specimen with marble inclusion.

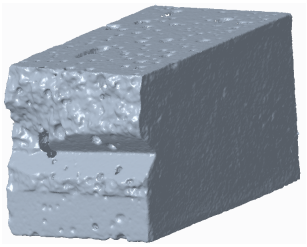

Fig. 6: Scanned surfaces of specimen with granite inclusion.

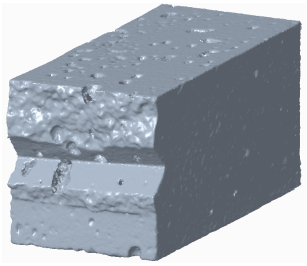

Fig. 7: Scanned surfaces of specimen with amphibolite inclusion.

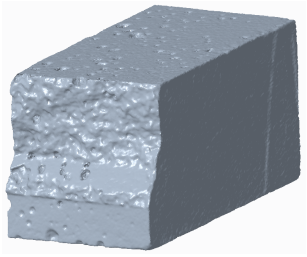

Fig. 8: Scanned surfaces of specimen with basalt inclusion.

4.3. Evaluation of fracture toughness

The measured F–d diagrams were used with the knowledge of real edge notch depth and specimen's height from 3D scanning to estimate the values of fracture toughness K_{Ic}.

Fracture toughness K_{Ic} represents a linear elastic brittle material's resistance to crack propagation and was estimated according to [10] as:

$$K_{\mathrm{Ic}} = \frac{6F_{\max}S}{4BW^2}\sqrt{a_0}\,Y\,(\alpha) \tag{1}$$

where $F_{\max}$ represents peak load in (kN), S is a load span in (mm), a_0 crack length in (mm), B thickness of specimen in (mm) and $Y(\alpha)$ shape function in (–) according to [11], see Eq. 2.

$$Y(\alpha) = \frac{1,99 - \alpha(1-\alpha)(2,15 - 3,93\alpha + 2,7\alpha^2)}{(1+2\alpha)(1-\alpha)^{3/2}} \tag{2}$$

Calculated fracture toughness $K_{\mathrm{Ic,d}}$ for designed notch depth $a_0 = 12$ mm and $K_{\mathrm{Ic,m}}$ for measured notch depth can be seen in Tab. 2.

Tab. 2: Calculated fracture toughnesses for specimens.

Specimen	MTX	MAR	GRA	AMP	BAS
$K_{\mathrm{Ic,d}}$(MPa $\cdot$ m$^{1/2}$)	0.590	0.436	0.400	0.337	0.424
$K_{\mathrm{Ic,m}}$(MPa $\cdot$ m$^{1/2}$)	0.555	0.397	0.366	0.314	0.390
$K_{\mathrm{Ic,m}}/K_{\mathrm{Ic,d}}$ (–)	**0.94**	**0.91**	**0.92**	**0.93**	**0.92**

The differences between fracture toughnesses $K_{\mathrm{Ic,d}}$ and $K_{\mathrm{Ic,m}}$ are approximately 10 % and thus are not negligible. In addition, the fracture toughness is overestimated when considering the design values.

4.4. Evaluation of specific fracture energy

Specific fracture energy G_{F} in (J/m^2) represents energy necessary for the creation of a unit area of crack [12], see Eq. 3.

$$G_{\mathrm{F}} = \frac{W_{\mathrm{F}}}{A_{\mathrm{lig}}} \tag{3}$$

where W_{F} is the work of fracture (area under the F–d diagram) in (N·mm), see Eq. 4, and A_{lig} represents area of ligament in (mm^2).

$$W_{\mathrm{F}} = \int_0^d F\mathrm{d}d \tag{4}$$

The area of ligament is usually calculated as a projection of the crack propagation path times the width of specimen. Nevertheless, if the crack propagation path is more complex, it is better to measure the area of ligament by 3D Scanner (or other technique). Also,

the value of calculated area of ligament will be, due to the complexity of fracture surfaces (which are in fact fractals), lower in comparison to the measured ones. These differences cause that the value of specific fracture energy evaluated from the calculated area of ligament $G_{F,c}$ will be in some cases higher in comparison to the specific fracture energy evaluated from the measured area of ligament $G_{F,m}$, see Tab. 3.

Tab. 3: Calculated specific fracture energy for specimens.

	MTX	MAR	GRA	AMP	BAS
W_F (N · mm)	56.4	63.0	41.5	38.4	42.5
$A_{lig,m}$ (mm^2)	1298.5	1300.7	1359.4	1349.7	1291.9
$G_{F,m}$ (J/m^2)	43.4	48.4	30.5	28.5	32.9
$A_{lig,c}$ (mm^2)	1150.3	1269.7	1355.5	1347.5	1261.7
$G_{F,c}$ (J/m^2)	49.0	49.6	30.6	28.5	33.7
$G_{F,m}/G_{F,c}$ (–)	0.9	1.0	1.0	1.0	1.0

The highest difference between $G_{F,m}$ and $G_{F,c}$ is in the case of the reference specimen. In the case of specimens with rock inclusion, the differences are not so significant due to the presence of caverns and cavities, which were not taken into account in the $A_{lig,m}$ measurements.

5. Conclusion

3D laser scanning is a progressively expanding technology for a wide range of applications in modern industry and quality control. In this paper, the 3D laser scanning is introduced for 3D shape capture of special designed specimens, to verify designed notch depth and specimen height and to measure the area of ligament. From the actual notch depth and specimen height obtained by 3D scanner, the fracture toughness was calculated and compared with the fracture toughness for designed notch depth. The differences between fracture toughnesses were approximately 10 %. In addition, the fracture toughness for designed notch depth is overestimated. Macrostructures of fracture surfaces also correspond to the results (values of fracture toughness). The most porous area of ligament and disruption of horizontal alignement of inclusion was found in the case of specimen with amphibolite inclusion, which corresponds to the lowest value of fracture toughness. On the contrary, the most compact areas of ligament were found in the case of specimens with marble and basalt inclusion, which also correspond to the highest values of fracture toughness.

The areas of ligaments were also measured and the values of specific fracture energy were evaluated for both areas of ligament – i) calculated as a projection of crack propagation path and ii) measured by 3D scanner. The highest difference between specific fracture energy evaluated from calculated and measured area of ligament is in the case of the reference specimen. In the case of specimens with rock inclusion, the differences are not so significant due to the presence of caverns and cavities, which were not taken into account in the measured area of ligament. However, in the case of reference specimens, the difference between specific fracture energy evaluated from calculated and measured area of ligament was approximately 10 %. In addition, the specific fracture energy evaluated from calculated area of ligament is overestimated.

Data from 3D scanning will be used in the next phase of the project to obtain fractal dimensions of fracture surfaces, similar to the publication [13]. The aim of the future work will be whether the walking divider method algorithm with an improvement [14] can also be used for data from 3D scanning, which differs from those obtain by a 2D profilometer.

Acknowledgment

This outcome has been achieved with the financial support of the Brno University of Technology under project No. FAST-J-22-8038. The author would also like to thank many kind colleagues who lent a helping hand.

References

[1] Eurocode 2. *Design of concrete structures: Part 1-1 : General rules and rules for buildings*. Brussel: European Committee for Standardization, second edition, 2011.

[2] FIB model code for concrete structures 2010. Berlin: Ernst, 2013, ISBN 978-3-433-03061-5.

[3] RANDL, N. Design recommendations for interface shear transfer in fib Model Code 2010. *Structural Concrete*. 2013, vol. 14, iss. 3, pp. 230–241. ISSN 1464-4177. DOI: 10.1002/suco.201300003.

[4] MEDŘICKÝ, R. and P. KELLER. 3D skenery pro použití v průmyslu. *AUTOMA: časopis pro automatizační techniku*. 2015, iss. 12, pp. 34–37. ISSN 1210-9592. Available at: https://automa.cz.

[5] TREBUŇA, P., M. MIZERÁK and L. ROSOCHA. 3D SCANING – TECHNOLOGY AND RECONSTRUCTION. *Acta Simulatio*. 2018, vol. 4, iss. 3, pp. 1–6. ISSN 1339-640. DOI: 10.22306/asim.v4i3.44.

[6] YALÇINKAYA, S., YILDIZ, B. and M. BORAK. OPTICAL 3D SCANNER TECHNOLOGY. In: *3rd International Congress on 3D Printing*

(Additive Manufacturing) Technologies and Digital Industry. Antalya, 2018, pp. 558–565. ISBN 978-605-68886-6-3.

[7] VYHLÍDAL, M., ROZSYPALOVÁ, I., MAJDA, T., DANĚK, P., ŠIMONOVÁ, H., KUCHARCZYKOVÁ, B. and Z. KERŠNER. Fracture response of fine-grained cement-based composite specimens with special inclusions. *Solid State Phenomena*. 2019, vol. 292, pp. 63–68. ISSN 1662-9779. DOI: 10.4028/www.scientific.net/SSP.292.63.

[8] VYHLÍDAL, M., ROZSYPALOVÁ, I., ŠIMONOVÁ, H., KUCHARCZYKOVÁ, B., VAVRO, L., VAVRO, M., NĚMEČEK, J., ROVNANÍKOVÁ, P. and Z., KERŠNER. Effect of petrographic composition and chemistry of aggregate on the local and general fracture response of cementitious composites. *Frattura ed Integrita Strutturale*. 2022, vol. 16, iss. 60, pp. 13–29. ISSN 1971-8993. DOI: 10.3221/IGF-ESIS.60.02.

[9] CREAFORM (AMETEK): HandySCAN3D SILVER Series, Proven and trusted professional 3D scanners at an accessible price. Available at: http://www.3d-skenovani.cz/wp-content/uploads/2021/03/HandySCAN3D_SILVER_Series_Brochure_EN_EMEA_20210127.pdf.

[10] KARIHALOO, B. L. *Fracture Mechanics and Structural Concrete*. Essex:Longman Scientific and Technical, 1995. ISBN 0-582-21582-X.

[11] SRAWLEY, J. E. Wide range stress intensity factor expressions for ASTM E 399 standard fracture toughness specimens. *International Journal of Fracture*. 1976, vol. 12, iss. 3, pp. 475–476. ISSN 0376-9429. DOI: 10.1007/BF00032844.

[12] RILEM TC-50 FMC. Determination of the fracture energy of mortar and concrete by means of three-point bend tests on notched beams. *Materials and Structures*. 1985, vol. 18, pp. 287–290. ISSN 1365-1609. DOI: 10.1007/BF02472918.

[13] SOBEK, J., FRANTÍK, P., TRČKA, T. and D. LEHKÝ. Fractal Dimension Analysis of Three-Point Bending Concrete Test Specimens. *MATEC Web of Conferences*. 2020, vol. 323, iss. 107, pp. 1–6. ISSN 2261-236X. DOI: 10.1051/matecconf/202032301011.

[14] FRANTÍK, P. An Approach for Accurate Measurement of Fractal Dimension Distribution on Fracture Surfaces. *Transactions of the VŠB - Technical University of Ostrava, Civil Engineering Series*. 2022, vol. 22, iss. 1, pp. 7–12. ISSN 1213-1962. DOI: 10.35181/tces-2022-0002.